Geosci. Instrum. Method. Data Syst., 6, 15–26, 2017
www.geosci-instrum-method-data-syst.net/6/15/2017/
doi:10.5194/gi-6-15-2017

Geoscientific Instrumentation Methods and Data Systems
Open Access
EGU

Time series analysis of ground-based microwave measurements at K- and V-bands to detect temporal changes in water vapor and temperature profiles

Sibananda Panda[1], **Swaroop Sahoo**[2], **and Govindan Pandithurai**[3]

[1]School of Electronics Engineering, KIIT University, Odisha, India
[2]Department of Electrical Engineering, Indian Institute of Technology Palakkad, Palakkad, Kerala, India
[3]Indian Institute of Tropical Meteorology, Pune, India

Correspondence to: Swaroop Sahoo (swaroop.sahoo769@gmail.com)

Received: 14 May 2016 – Published in Geosci. Instrum. Method. Data Syst. Discuss.: 1 July 2016
Revised: 10 November 2016 – Accepted: 15 November 2016 – Published: 18 January 2017

Abstract. Ground-based microwave measurements performed at water vapor and oxygen absorption line frequencies are widely used for remote sensing of tropospheric water vapor density and temperature profiles, respectively. Recent work has shown that Bayesian optimal estimation can be used for improving accuracy of radiometer retrieved water vapor and temperature profiles. This paper focuses on using Bayesian optimal estimation along with time series of independent frequency measurements at K- and V-bands. The measurements are used along with statistically significant but short background data sets to retrieve and sense temporal variations and gradients in water vapor and temperature profiles. To study this capability, the Indian Institute of Tropical Meteorology (IITM) deployed a microwave radiometer at Mahabubnagar, Telangana, during August 2011 as part of the Integrated Ground Campaign during the Cloud Aerosol Interaction and Precipitation Enhancement Experiment (CAIPEEX-IGOC). In this study, temperature profiles for the first time have been estimated using short but statistically significant background information so as to improve the accuracy of the retrieved profiles as well as to be able to detect gradients. Estimated water vapor and temperature profiles are compared with those taken from the reanalysis data updated by the Earth System Research Laboratory, National Oceanic and Atmospheric Administration (NOAA), to determine the range of possible errors. Similarly, root mean square errors are evaluated for a month for water vapor and temperature profiles to estimate the accuracy of the retrievals. It is found that water vapor and temperature profiles can be estimated with an acceptable accuracy by using a background information data set compiled over a period of 1 month.

1 Introduction

Water vapor along with temperature affects various atmospheric processes, particularly cloud formation, initiation of convective storms (Trenberth et al., 2005) and tropical cyclones (Needs, 2009; Ali, 2009). Therefore, accurate information about their spatial and temporal distribution as well as variation in the lower troposphere is essential for the initialization of numerical weather prediction models, which in turn improves the forecast of various weather events (NRC, 2009).

Various instruments are used to measure water vapor and temperature profiles in the lower troposphere, i.e., radiosondes, Raman lidar and microwave radiometer. Radiosondes are by far the main source of water vapor and temperature profiles information for numerical weather prediction. The measured profiles have a vertical resolution of approximately 10 m in the lowest 3 km of troposphere but are launched once or twice a day at most sites around the world (Wang et al., 2008). Therefore, they cannot be used to detect the temporal variations and gradients in the atmospheric humidity and temperature profiles at regular intervals of time and space. Raman lidars (Goldsmith et al., 1998) and differential absorption lidars (DIAL) (Spuler et al., 2015) are also used during clear sky conditions for sensing humid-

ity profiles with a vertical resolution comparable to that of a radiosonde from ground to an altitude of 3 km. Since lidars are quite expensive, they cannot be deployed in a dense network to provide information on spatial distribution and variation on water vapor and temperature. In addition to these instruments, microwave radiometers, both ground-based and airborne, operating in the 20–60 and 166–190 GHz ranges are used for the retrieval of water vapor, temperature and liquid water profiles. Ground-based microwave radiometers have been designed, fabricated and used to sense water vapor and temperature profiles from ground to 10 km altitude (Iturbide-Sanchez et al., 2007; Solheim, et al., 1998). Satellite-based instruments like Advanced Microwave Sounding Units (AMSU-A and B) on board NOAA-15 (Susskind et al., 2011; Rosenkranz, 2001) as well as Sondeur Atmospherique du Profil d'Humidité Intertropicale par Radiometrie (SAPHIR) Microwave Analysis and Detection of Rain and Atmospheric Systems (MADRAS) on board the Megha-Tropiques (Rao, et al., 2013) have been used to retrieve humidity and temperature profiles in addition to a range of other parameters. The AMSU-A and B channels operate close to the 22.235, 60 and 183 GHz absorption lines as well as at the 89 GHz window frequency. In addition to these instruments a mini-satellite flower constellation of millimeter-wave radiometers for atmospheric observations known as FLORAD operates at frequencies close to the 89, 118 and 183 GHz to estimate water vapor, temperature, cloud liquid content and precipitation rate (Marzano, et al., 2009). Both the ground-based and airborne microwave radiometers have a fine temporal resolution ranging from a few millisecond to a few minutes depending on the integration time of the measurement channel. However, radiometers have a variable vertical resolution and accuracy depending on the thermodynamic property being retrieved.

Humidity and temperature profiles have been retrieved from microwave radiometer measurements by Westwater (Westwater, 1993) using various retrieval techniques while Scheve (Scheve et al., 1999) used the minimum variance estimation technique. Sahoo (Sahoo et al., 2015b) used the Bayesian optimal estimation technique while focusing on sensing the gradients and temporal changes associated with water vapor profiles retrieved by using K-band radiometer measurements and an optimized background data sets.

The novel feature of the work discussed in this paper is the estimation of water vapor density and temperature profiles within certain limits of accuracy while detecting temporal variations and gradients in the profiles. The profiles are estimated by inverting K- and V-band measurements using the Bayesian algorithm along with a background data set compiled over a period of 1 month. The background data set compiled for a period of 1 month is specific to the time period of radiometer measurements and conforms to the weather conditions during that period. This method results in a significant improvement of accuracy over the normal method of using a large data set collected for a long period of time (usually 3–4 years). However, the improved results discussed in this paper are specific for a location and the method needs be adapted for a particular region.

The Bayesian optimally estimated profiles are then compared with profiles estimated using the neural network (NN) method as well as profiles taken from the reanalysis data from Earth System Research Laboratory, National Oceanic and Atmospheric Administration (NOAA). Here, the reanalysis data are considered as truth and the error in this study is the difference between the radiometer retrieved profiles (using both neural network and Bayesian optimal estimation) and those from the reanalysis data.

2 Instruments deployment

Indian Institute of Tropical Meteorology (IITM) had deployed a microwave radiometer in Mahabubnagar (16°44′ N, 77°59′ E), Telangana, for the whole month of August 2011 as part of the Integrated Ground Campaign during the Cloud Aerosol Interaction and Precipitation Enhancement Experiment (CAIPEEX-IGOC) (Leena et al., 2015). This is a frequency agile radiometer and operated at 8 frequencies in the range 22–30 GHz and 14 frequencies from 51.0 to 58.0 GHz in V-band, at elevation angles of 15, 90 and 165°. The resolution of the instrument varies from 0.1 to 1 K depending on integration time, i.e., 0.01 to 2.5 s (Radiometrics Corporation, 2008). The accuracy of the brightness temperature measurements is approximately 0.2 K and the bandwidth of the channels is 300 MHz. This instrument also has a single channel infrared radiometer in addition to surface pressure, humidity and temperature sensors. The multichannel microwave radiometer is calibrated by injecting noise from a noise diode to remove the system gain fluctuations. Two sided tipping curve calibration method has been used to determine the brightness temperatures from the measured voltages for water vapor channels and the cold (liquid nitrogen) and hot load calibration (internal black body at ambient temperature) is used to calibrate the temperature channels measurements.

Radiometer measurements during the field campaign were performed throughout day and night under varying atmospheric conditions which included clear and cloudy skies. The time series of calibrated brightness temperatures for 22.23, 25.0, 51.243 and 53.36 GHz are shown in Fig. 1. It can be observed that brightness temperatures at 22.23 GHz are comparatively higher than those at 25 GHz. This is because 22.23 GHz is the water vapor resonance frequency and is more sensitive to water vapor in the atmosphere than 25 GHz, which is significantly far away from the water vapor resonance frequency. Similarly, measurements at 53.36 GHz are higher than those at 51.243 GHz because of the proximity of 53.36 GHz to the oxygen complex. Thus, measurement frequencies are sensitive to water vapor and temperature to a varying extent as explained in Sect. 3.1. This can also be confirmed by analyzing the weighting functions correspond-

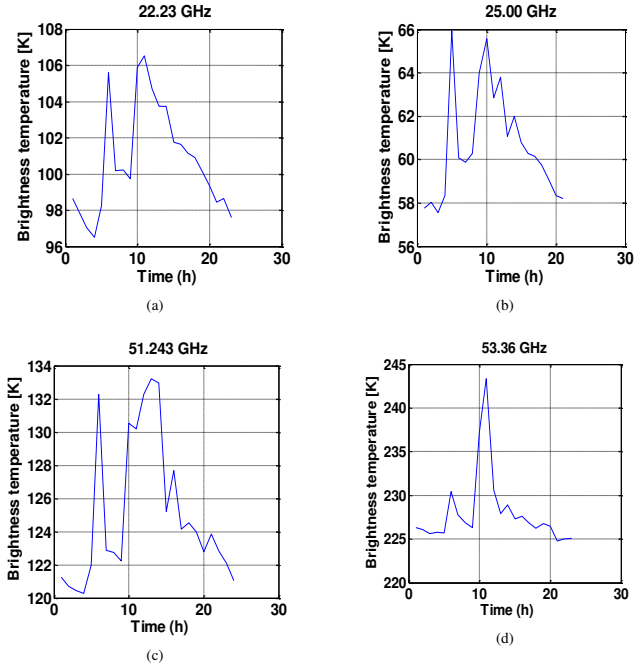

Figure 1. Time series of brightness temperature at 22.23, 25.0, 51.243 and 53.36 GHz.

ing to water vapor and temperature frequencies shown in Fig. 2. Figure 2a shows that weighting function values for 22.234 GHz are higher than those at 25.00 GHz at altitudes above 2 km while weighting function values at 25 GHz have slightly higher values than those at 22.234 GHz below 2 km. This is because the measurements at 22.234 GHz are comparatively more sensitive to changes in water vapor at altitudes above 2.5 km while those at 25.00 GHz are more sensitive to changes in water vapor below that altitude. However, the weighting function values at 22.234 GHz for altitude range 2.5–8 km are significantly higher than those at 25.00 GHz so that brightness temperatures at 22.234 GHz are still higher than those at 25.00 GHz.

The temperature measurement frequencies shown in Fig. 2b are most sensitive to temperature variations from 0 to 4 km altitude. The 53.36 GHz weighting function (represented by green line in Fig. 2b) is higher than 51.248 GHz weighting function (represented by blue line in Fig. 2b) at all altitudes.

To complement the radiometer measurements, Vaisala RS92-SGP radiosondes were launched everyday at 12:00 UTC. These radiosondes were launched from the radiometer deployment location to provide vertical profiles (with temporal resolution of two seconds) of relative humidity, temperature, dew point temperature, pressure and wind. These radiosondes data have been used as the source of a-priori information as well as the source of background data set during this study and analysis, as explained in Sect. 3.2.

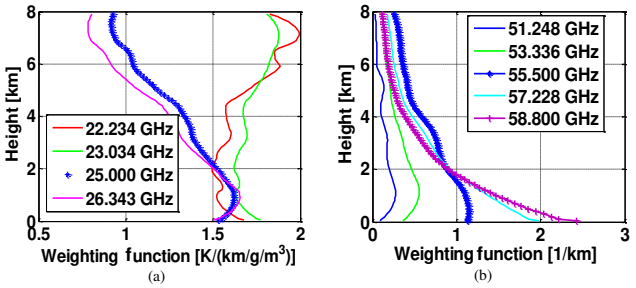

Figure 2. (a) Weighting functions for measurement frequencies used for water vapor profile retrieval. **(b)** Weighting functions for measurement frequencies used for temperature profile retrieval.

3 Theoretical background

3.1 Remote sensing of water vapor and temperature profile

Remote sensing of water vapor and temperature is based on the measurement of microwave radiation emitted by water vapor and oxygen molecules. The emission and absorption of microwave radiation due to water vapor and oxygen in each tropospheric layer causes the change in microwave radiation that reaches the ground. This variation in radiation is due to the concentration of water vapor in the atmosphere and the temperature at various altitudes. Therefore, this microwave radiation reaching the ground is source of information about the humidity distribution and temperature variation in the atmosphere at different heights.

Measurement of this radiation at the weak water vapor absorption line (centered at 22.235 GHz) is used for the sensing of water vapor profile variation. This is based on humidity absorption line pressure broadening. This broadening is due to motion of the water molecules and their collisions with other water vapor molecules. Thus change in pressure has a significant impact on the width of the absorption lines as well as the absorption values. Therefore, a decrease in the atmospheric pressure (at high altitudes) results in reduction of the line width and increase of the water vapor absorption line strength, which is most prominent at 22.235 GHz (the center of the absorption line). Therefore, the closer the proximity of the measurement frequency is to the weak water vapor resonance frequency, the higher the sensitivity to water vapor at high altitudes. As the pressure increases the absorption line widens, resulting in reduced sensitivity of resonance frequency measurements to water vapor at high altitudes. However, frequencies farther away from the center frequency are more sensitive to water vapor changes close to ground level. This is again proven by the weighting functions values at various frequencies. Weighting functions closest to the water vapor resonance frequencies are almost twice more sensitive to water vapor at 8 km than the weighting function farther away from the resonance frequency. Frequencies further

away from the resonance peak are most sensitive to changes close to ground level. Therefore, a combination of various frequency measurements is able to detect the profile information about water vapor.

Similarly, microwave radiation from oxygen at the 60 GHz absorption complex can be used for retrieving temperature profile information because atmospheric absorption in the 50–75 GHz range is primarily due to oxygen molecules. The oxygen absorption line between 51.5 and 67.9 GHz (Rosenkranz 1993) is primarily due to the magnetic moment 33 spin-rotational lines. These spin-rotational lines merge together at lower altitude to form a pressure broadened line which has a shape similar to an absorption band centered at 60 GHz. However, the oxygen absorption line intensity is not the result of simple addition of isolated line intensities but rather the "overlap interference" which gives rise to a very complex absorption band called the oxygen complex. This oxygen complex results in the opacity at 60 GHz being significantly higher than that at 50 GHz, so a ground-based radiometer measuring at 60 GHz just observes the radiation emitted close to the ground surface. Thus, to sample the temperature at various altitudes of the troposphere, measurements need to be performed at a number of frequencies away from the center frequency.

Since oxygen is the most uniformly mixed gas in the atmosphere and its proportion in the lower atmosphere is almost constant and altitude independent from ground level to 80 km, the microwave radiation at the oxygen absorption lines contain atmospheric temperature profile information.

3.2 Retrieval techniques

3.2.1 Bayesian optimal estimation

The Bayesian optimal estimation is an inversion method which uses multiple K- and V-band microwave frequency measurements to retrieve profiles of humidity and temperature. This retrieval of water vapor and temperature profiles from brightness temperature measurements is a nonlinear and ill-posed problem. To overcome the ill-posed problem Bayesian optimal estimation retrieval technique uses a priori humidity and temperature information as well as background information covariance matrix as constraint to determine a unique solution to the inverse problem. A priori in this paper represents the measurement of water vapor and temperature profiles prior to the radiometer brightness temperature measurements. This is also known as the initialization profile in this paper. The a priori information is taken from radiosonde launched a few hours before the radiometer performs the measurement.

In addition to the a priori information, water vapor density and temperature background information statistics are also used. Background information statistics here mean the background information covariance information represented by the matrix $\overline{\overline{S}}_a$ as discussed later in this section. This matrix provides variability information associated with the atmospheric humidity and temperature profiles as well as the inter-layer correlation for a particular time period. The number of elements in the background data set and the relationships among them determines the values of the background information covariance matrix elements. Since in this study the data set used for calculating the background statistics has been taken close to measurement time, it will be more representative of weather conditions during that time period and location.

The Bayesian optimal estimation uses the Levenberg–Marquardt (LM) optimization method (Rodgers, 2000) given in Eq. (1).

$$\bar{x}_{i+1} = \bar{x}_i + \left((1+\gamma)\,\overline{\overline{S}}_a^{-1} + \overline{\overline{K}}_i^{T}\,\overline{\overline{S}}_\epsilon^{-1}\,\overline{\overline{K}}_i\right)^{-1} \left(\overline{\overline{K}}_i^{T}\,\overline{\overline{S}}_\epsilon^{-1}\left[\bar{T}'_{\mathrm{B}} - \bar{T}_{\mathrm{B}}(\bar{x}_i)\right] - \overline{\overline{S}}_a^{-1}\left[\bar{x}_i - \bar{x}_a\right]\right), \quad (1)$$

where i is the iteration index, $\overline{\overline{K}}_i$ is the kernel or weighting function matrix and determines the sensitivity of the measurements at various frequencies to changes in the parameter of interest at various altitudes, $\bar{x}_i$ is the water vapor density or temperature profile which is updated at each iteration and is same as initialization profile for $i = 1$, $\bar{T}'_{\mathrm{B}}$ is the measured brightness temperature vector at water vapor density or temperature measurement frequencies and $\bar{x}_{\mathrm{a}}$ is the a priori profile and is same as the initialization profile in this case because a small data set is used as background data set. $\bar{T}_{\mathrm{B}}(\bar{x}_i)$ is the radiative transfer model simulated brightness temperature using the absorption coefficients calculated from a Rosenkranz model (Rosenkranz, 1993, 1998).

$\overline{\overline{S}}_\epsilon$ is the observation error covariance matrix and contains the uncertainty information associated with the measurement. The observation error covariance matrix takes into consideration the radiometric measurement noise (E), representativeness error (M) and radiative transfer model errors (F). Radiometric noise is determined based on radiometric resolution, which is the minimum difference in scene brightness temperature that can be sensed by the receiver. This value for MP3000-A varies from 0.1 to 1 K depending on integration time (Radiometrics Corporation, 2008). The typical value is 0.25 K for each measurement frequency while considering an integration time of 250 ms. In addition to the radiometric noise, forward model errors are introduced due to inadequate absorption models. These are determined using the difference between brightness temperatures simulated by two absorption models, i.e., the Rosenkranz model and MPM93 (Liebe et al., 1993). Another source of uncertainty is the representativeness error, which takes into consideration the radiometer's sensitivity to fluctuations in the atmosphere on a time scale shorter than what can be represented by any numerical weather prediction model or radiosondes profiles.

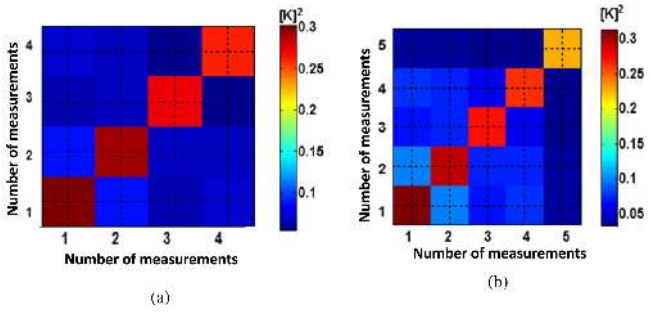

Figure 3. The observation error covariance matrix for **(a)** water vapor frequency measurements **(b)** temperature measurements.

The representative covariance is calculated in Eq. (2).

$$M = E\left(\bar{T}'_{\mathrm{B}}(t+\Delta t) - \bar{T}'_{\mathrm{B}}(t)\right)\left(\bar{T}'_{\mathrm{B}}(t+\Delta t) - \bar{T}'_{\mathrm{B}}(t),\right)^{T} \quad (2)$$

where t is time and Δt is the time scale of difference. The observation error covariance matrix is shown in Fig. 3, where the axes represent the number of measurement frequencies. The diagonal elements of the observation error covariance matrix are approximately in the range of 0.23 to 0.29 K^2 and some of the off-diagonal elements are close to zero.

$\overline{\overline{S}}_{\mathrm{a}}$ is the background covariance matrix, which is computed using information from 50 radiosonde profiles launched over a period of 1 month. γ is the LM factor and its value is updated at each iteration based on value of $J(x)$ from Eq. (3). Various initial values of γ in the range of $\gamma = 1$ and $\gamma = \infty$ have been considered for starting of the iteration. For $\gamma = 1$, the iteration might move towards a local minima while in case of $\gamma = \infty$ the iteration immediately moves towards the global minima, which gives a solution that does not converge. Therefore, the initial value of γ is assumed to be 1. It is observed that the algorithm does not converge with a valid output for this initial value of gamma so the initial value of gamma is increased at regular intervals to check the convergence. It is found empirically that gamma with an initial value of 5000 converges the algorithm for all cases. As part of the iteration, if the value of $J(x)$ increases, then the iteration is discarded and the value of γ is increased 10 fold and the iteration is repeated. This is done so as to discard any invalid output which could be close to one of the local minima. If value of $J(x)$ decreases, then the iteration is valid and the value of γ is reduced by a factor of 2 for the next iteration even if the convergence criteria is not satisfied, i.e., Eq. (4) (Hewison, 2007). This process is followed until the convergence criterion given by Eq. (4) is validated by the output profile. The normalized cost function and gamma values are shown in Fig. 4. It can be observed that as the cost function decreases, the gamma value decreases and vice versa.

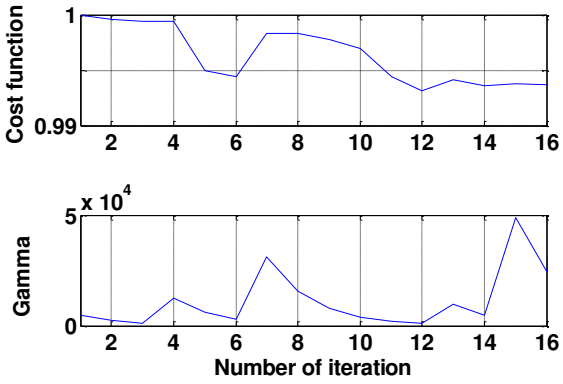

Figure 4. The value of normalized cost function and gamma with respect to number of iterations are shown in the top and bottom figure, respectively.

LM technique output is dependent on the cost function represented by $J(x)$ in Eq. (3):

$$J(x) = \left[\bar{x} - \bar{x}^{\mathrm{b}}\right]^{T} \overline{\overline{S}}_{\mathrm{a}}^{-1} \left[\bar{x} - \bar{x}^{\mathrm{b}}\right] + \left[\bar{T}_{\mathrm{B}}(\bar{x}_i) - \bar{T}_{\mathrm{B}}{}'\right]^{T} \overline{\overline{S}}_{\epsilon}^{-1} \left[\bar{T}_{\mathrm{B}}(\bar{x}_i) - \bar{T}_{\mathrm{B}}{}'\right], \quad (3)$$

where $\bar{x}^{\mathrm{b}}$ and $\bar{x}$ are the initialization profiles (either water vapor or temperature) and output profile (either water vapor or temperature) for each iteration, respectively. The final water vapor or temperature output profiles are determined by the convergence criterion given by Eq. (4):

$$\left[\bar{T}_{\mathrm{B}}(\bar{x}_{i+1}) - \bar{T}_{\mathrm{B}}(\bar{x}_i)\right]^{T} \overline{\overline{S}}_{\delta y}^{-1} \left[\bar{T}_{\mathrm{B}}(\bar{x}_{i+1}) - \bar{T}_{\mathrm{B}}(\bar{x}_i)\right] \ll m, \quad (4)$$

where m is 5 and 7 (dimension of water vapor and temperature measurement vector) for water vapor and temperature profile retrieval and $\overline{\overline{S}}_{\delta y}$ is the covariance between $\bar{T}'_{\mathrm{B}}$ and $\bar{T}_{\mathrm{B}}(\bar{x}_{\mathrm{i}})$. Equation (4) determines the termination of the iterative process. The iteration stops when Eq. (4) reaches the value q, which is very small in comparison to m. Therefore, the value of q is chosen to be 0.05 and 0.07 for water vapor and temperature profile retrieval, respectively, which is $1/100$ times the number of measurements used.

3.2.2 Impact of background data set on retrieval

As already studied and determined by Scheve (1999), Hewison (2007), Solheim et al. (1998) and Sahoo et al. (2015a), the number of measurement frequencies which provide altitude related information about water vapor and temperature is limited by the information content or degrees of freedom of the measurements. Thus, use of these measurements in various inversion methods to retrieve the thermodynamic properties at more number of altitudes than the information content limit is an ill-posed as well as a nonlinear problem. To overcome these shortcomings, Bayesian optimal estimation method uses background information statistics.

Background information statistics here mean the background covariance information represented by the matrix $\overline{\overline{S}}_a$. The background data set is very important for the performance of the retrieval algorithm in terms of accuracy and ability to sense temporal changes. This is because it determines the range of variability information associated with water vapor or temperature profiles during a time period. Thus the background data set taken closer in time to the radiometer measurement will describe the atmospheric conditions, i.e., the temperature and humidity profiles during the measurements while background data set taken over a long period (1 year or so) of time will take into consideration the variability information for the whole year and hence will over shadow variability information which might be more useful in a short period of time.

The atmospheric conditions during a particular season or month are correlated because the atmospheric conditions are similar throughout the time period accept a few outliers which cannot be correlated to the time of interest. Therefore, measurements along with the background data set and the a priori will retrieve the most probable water vapor and temperature profile while an outlier might or might not be detected depending on whether that event is properly described by the background covariance matrix.

The background information covariance matrix used in this paper is shown in Fig. 5a and b, calculated using water vapor density and temperature profiles, respectively, which have been measured over a period of 1 month. It can be observed from Fig. 5a that most of the water vapor variability information is between 20 and 40 layers, which correspond to the altitude range of 2–4 km. However, Fig. 5b shows that the temperature variability information is primarily below altitude of 1 km and also in the range of 2–4.2 km. In contrast to these results, when background information covariance matrix is computed from a large data set, important weather events or temporally varying conditions are overshadowed because the covariance matrix takes into consideration the overall variability information while reducing the weight of certain weather conditions which correspond to a particular season (Sahoo et al., 2015b).

The goal of this study is to retrieve water vapor and temperature profiles with improved accuracy while using a background data set measured over a period of 1 month so as to detect the temporal changes and gradients in the lowest 8 km of the profiles.

3.3 Neural network estimation

Estimation of water vapor and temperature profiles from microwave radiometer brightness temperatures is done using a proprietary NN method developed by Radiometrics Corporation (Solheim, et al., 1998). NN zenith estimation of temperature, water vapor density profiles, relative humidity profiles and liquid water content is performed at a time from the microwave measurements as well as the infrared channel measurements. The retrieved profiles are estimated at 58 height levels at every 50 m steps from the surface up to 500 m, then at every 100 m steps to 2 km, and then the step size is increased to 250 m from 2 to 10 km. However, it has to be noted that above approximately 7 km, the atmospheric water vapor density and temperature approach the climatological mean values.

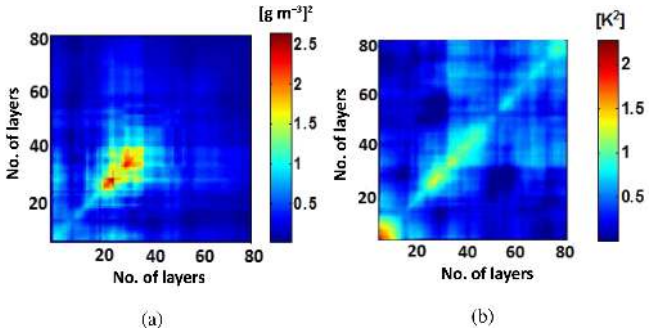

Figure 5. Background information covariance matrix for 80 layers (each layer is 100 m thick): **(a)** water density and **(b)** temperature profiles. The x and y axes are in kilometers for both the figures.

As part of the retrieval process the training of the NN is performed using a back-propagation algorithm and radiosonde data which have been collected over a period of time, i.e., usually 4 to 5 years. The radiosonde data used for training the network are taken from one or more sites which have climatological conditions similar to the observation site. The radiosonde profiles are used for simulating the brightness temperature using absorption models and radiative transfer equations. The NN estimation uses a standard feed-forward network (Radiometrics Corporation, 2008) to retrieve the temperature, humidity and liquid water profile that is most consistent with the atmospheric conditions and radiometric measurements.

However, in this case sufficient radiosonde profiles were not available for Mahabubnagar, so a slightly different approach was used in this study for neural network estimation of profiles. Radiosonde profiles were still used as training data set but these were taken from areas which had similar weather conditions and same altitude and latitude (but different longitude) as Mahabubnagar, Telangana. However, two sites at the same altitude and longitude may have significantly different weather depending on the general conformation of the mountains in the area, the marine currents as well as the advection processes. This could lead to biases in the training of the radiometer algorithm which in turn would increase the error of the retrieved profile.

4 Retrieval of atmospheric profiles

The Bayesian optimal estimation and NN zenith estimation methods are applied to the zenith microwave measurements

to estimate water vapor density and temperature profiles from ground to an altitude of 8 km in the troposphere for various days and times. The Bayesian optimal estimation method requires an initialization profile which is taken from radiosondes launched every day at 12:00 UTC. The initialization profiles from radiosondes are vertically averaged to correspond to 100 m layer thickness of retrieval. In addition to the measurements and initialization profile, background information covariance matrix is also required, which is calculated from the data set of radiosonde profiles launched during the experiment and is shown in Fig. 5. The retrieved profiles are compared with those from NOAA reanalysis data. The reanalysis profiles have water vapor and temperature samples at varying pressure levels. Therefore, these profiles are made uniform by interpolation so as to have samples at every 100 m interval from ground to 8 km above ground level.

4.1 Water vapor profiles

Water vapor profiles estimated using the Bayesian optimal estimation and NN method are shown in Fig. 6, along with the reanalysis data from NOAA. It can be observed that Bayesian optimal estimation performs better than the NN in estimating water vapor profile on all the days considered. The Bayesian optimal estimation is able to detect the variation in the profiles, which are smoothed by the NOAA data because of the coarse vertical resolution. The retrieved profile in Fig. 6a shows that both the Bayesian and NN zenith estimated water vapor profiles have similar performance on 7 August 2011 when the errors are in the range of 1.5–2.5 g m^{-3} from ground to 3 km above ground level. However, for 16 August 2011 the Bayesian and NN zenith retrieval errors are in the ranges of 0–1.5 and 0–3 g m^{-3}, respectively, as shown in Fig. 6b. The Bayesian retrieved profiles show significantly improved performance on 25 and 26 August 2011 and have errors less than 1.5 g m^{-3} in the lowest 2 km of the troposphere, which is better than the error associated with the NN zenith estimated profiles. It can also be observed from Fig. 6 that at the altitude range of 3–7 km, Bayesian optimal estimation method has an error less than 0.8 g m^{-3} for all cases except for 25 August 2011. Thus the NN zenith retrieval has a slight negative bias in the lowest 2 km of the troposphere.

In addition to the higher accuracy, Bayesian optimal estimation has been able to detect the gradient in the lowest 4 km of troposphere on 7, 16 and 25 August 2016, which is not observed in the reanalysis data. This detection of gradients in the water vapor density profiles is significant because water vapor is highly variable in the lowest 3 to 4 km of the troposphere, which greatly affects the evolution of the weather changes. The statistical analysis for profiles retrieved by Bayesian optimal estimation and NN is discussed in Sect. 4.3.

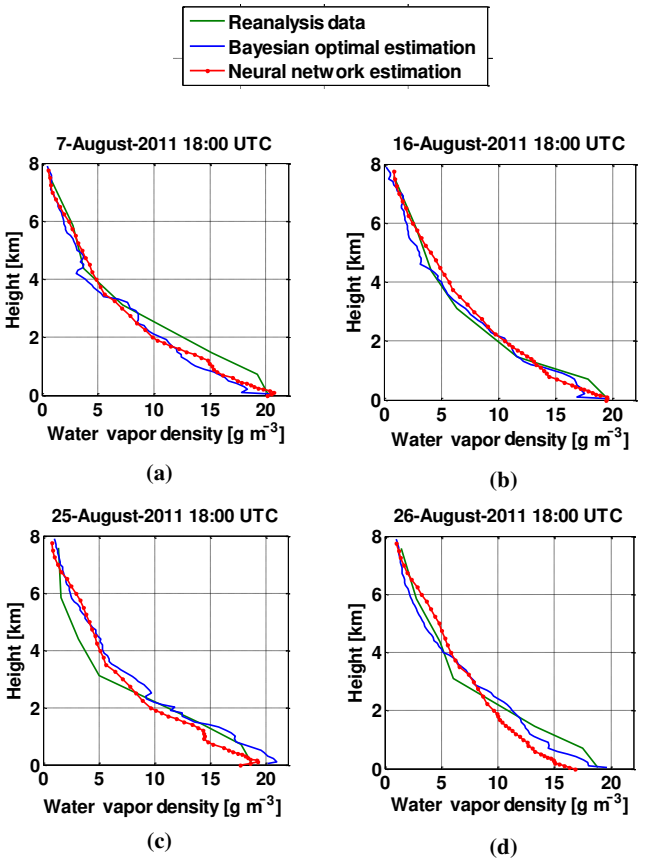

Figure 6. Time series analysis data of water vapor retrieved profiles.

4.2 Temperature profiles

Temperature profiles were estimated using both the estimation methods (Bayesian and NN methods) and have been shown in Fig. 7. The Bayesian method outperforms the NN estimated profile on all the days considered here. For altitudes below 3 km, the Bayesian optimal estimation has an error range of 0–1.5 K, and for altitudes above 4 km the Bayesian method error is less than 3 K for most of the cases considered in Fig. 7. The NN estimated profile consistently shows a negative bias when compared with the reanalysis data at all altitudes. However, the negative bias is more significant at 3 km and above where the NN error is higher than 6 K.

It can be noted that some of the fine changes and gradients in the temperature profile in the altitude range of 0–3 km are sensed by the Bayesian estimated temperature profile. The ability to sense gradients and temporal changes in the temperature profile are because of the background covariance matrix, which has been computed using a data set compiled over 1 month during the measurement time. This data set is correlated to the radiometer measurements because the radiosondes data have been taken over the time period of the ra-

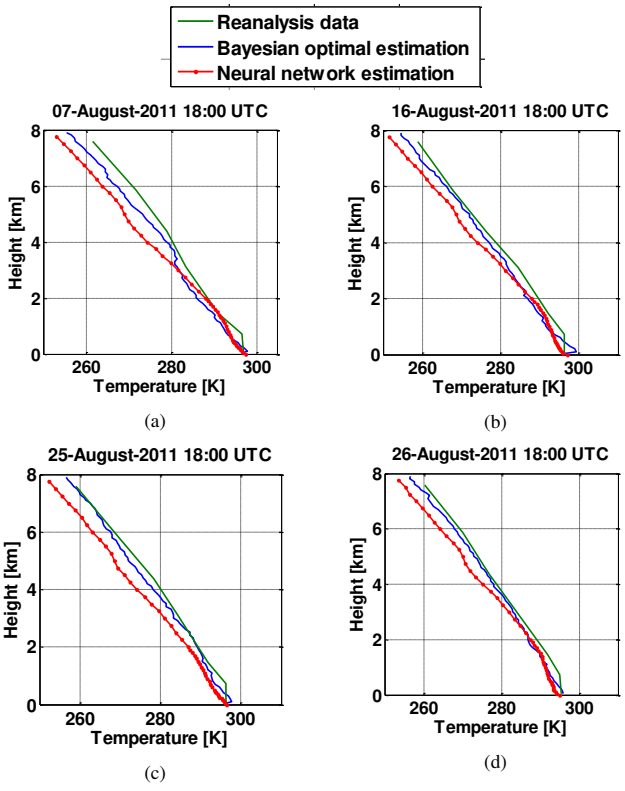

Figure 7. Time series analysis data of temperature retrieved profiles.

diometer measurements. The statistical analysis for Bayesian optimal estimation and NN zenith is discussed in Sect. 4.3.

4.3 Error analysis

To analyze the performance of both the retrieval techniques, the retrieval errors are calculated as the difference between the estimated (using either the NN or the Bayesian optimal estimation) and the reanalysis profiles. The range of errors associated with the water vapor profiles estimated using NN and Bayesian optimal methods are shown in Fig. 8a and b, respectively. Figure 8a shows that the errors for NN estimation in the lowest 2 km of the troposphere are in the range of -4.5 to $4\,\mathrm{g\,m^{-3}}$ and as the altitude increases the error range decreases and reduces to -2 to $2\,\mathrm{g\,m^{-3}}$ at 4 km above ground level. However, the range of errors associated with the Bayesian optimal estimation are -1 to $1\,\mathrm{g\,m^{-3}}$ at all altitudes for most of the cases as shown in Fig. 8b. Thus, the error associated with the Bayesian optimal estimation is significantly less than that of the NN algorithm particularly for water vapor profile retrieval. It can also be observed that the errors in most of the cases are less than zero for both the retrieval methods. This is because of the estimated profile being less than the reanalysis profile in most of the cases (thus the negative bias). In addition to that, it can be observed

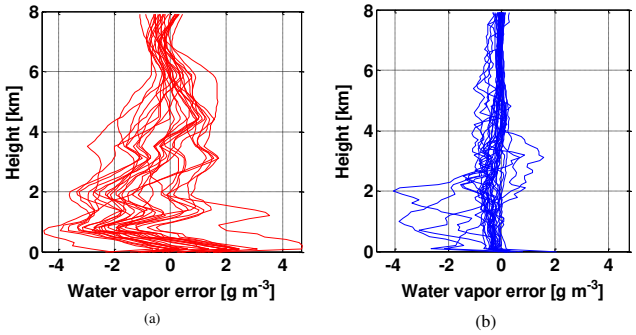

Figure 8. Error associated with water vapor density profile retrieved by **(a)** neural network and **(b)** Bayesian optimal estimation.

that some of the retrieved profiles in Fig. 8b showed higher than usual absolute errors, i.e., $2\,\mathrm{g\,m^{-3}}$ and above. This is because the water vapor profile retrieval accuracy is significantly affected by the a priori profile as shown by Sahoo et al. (2015). If the atmospheric conditions during the a priori profile measurement (radiosonde launch) are very different from the conditions during the radiometer measurements then the actual profile will be different from the a priori. This will result in errors which are higher than when the a priori and estimated profiles are similar or the weather conditions for the two times are not very different. This difference in weather conditions is due to a weather phenomenon or a rain event.

The range of errors associated with the temperature profiles are shown in Fig. 9a and b for both the NN and Bayesian optimal techniques, respectively. The error associated with the neural network profile is in the range of -3 to 5 K in the lowest 1 km of the troposphere and then the range changes to -4 to -8 K at 4 km above ground level. It is clear that the NN zenith retrieval underestimates the value of the temperature profile. The error associated with the Bayesian optimal estimated profile is shown in Fig. 9b and is in the range of -1 to 0 K except in the case of a few profiles. As in the case of water vapor profile, the errors associated with temperature profiles by Bayesian optimal estimation are significantly less than NN estimated profiles. The Bayesian optimally estimated retrievals using radiometer observations compare well with the reanalysis data because of the retrieval being constrained by a-priori and surface measurements provided by the radiometer.

Another analysis was performed to determine the sensitivity of retrieved profile to changes in elements of observation error covariance matrix in the Bayesian optimal estimation. Water vapor and temperature profiles already retrieved for various days as shown in Figs. 6 and 7 have been reanalyze after increasing the diagonal element of the observation error covariance matrix by $0.25\,\mathrm{K^2}$. The retrieved profiles for water vapor and temperature for both the observation error covariance matrices are shown in Fig. 10. It can be observed

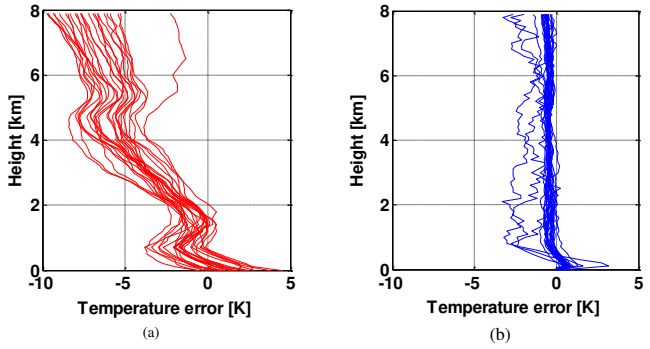

Figure 9. Error associated with temperature profiles retrieved by **(a)** neural network and **(b)** Bayesian optimal estimation.

that the retrieved water vapor profile for the modified covariance matrix has higher error than the profile retrieved using the covariance matrix shown in Fig. 3. The increase in error for the retrieved water vapor profile is in the range of 0.3 to 1.9 g m^{-3} (0 to 8 km altitude). Similarly, the increase of 0.25 K^2 in the diagonal elements of the temperature observation covariance matrix shown in Fig. 3 results in an increase of the temperature profile error by 0.2 to 0.5 K (0 to 8 km altitude) as shown in Fig. 10. Thus, the observation error covariance matrix has a significant impact on the retrieved profile quality and accuracy.

Additional analysis was performed to determine the deviation of the retrieved profiles from the NOAA reanalysis profile. Root mean square (RMS) errors are calculated for both the Bayesian and NN methods. RMS errors are calculated by comparing radiometer retrieved humidity and temperature profiles (retrieved using both Bayesian optimal estimation and NN method) with the reanalysis data (which is used as truth in this case).

Figure 11a shows the RMS error associated with Bayesian optimal and NN estimated water vapor profile. Bayesian retrieval error varies from 0.2 to 0.4 g m^{-3} in the lowest 4 km of the troposphere and is less than 0.2 g m^{-3} above 5 km altitude. In contrast, RMS error for NN retrieved profile is in the range of 1–2.5 g m^{-3} in the lowest 2 km of troposphere and is less than 1 g m^{-3} above 4 km. Thus, the RMS error for water vapor profile retrieved using Bayesian optimal estimation is less than NN.

Figure 11b shows the RMS error for Bayesian optimal and NN estimated temperature profiles. The RMS error associated with the Bayesian optimal estimated profile is less than 0.6 K at any altitude from 0 to 8 km above ground level. However, the NN zenith retrieval error range is 1–2 K for lowest 2 km and then increases consistently above 2 km. The maximum error is approximately 7.5 K at 8 km above ground level. Thus, the Bayesian retrieval algorithm performs significantly better than NN zenith for estimating temperature profile.

It is observed that the RMS error for NN estimated water vapor density profile has a decreasing behavior with altitude whereas the temperature profile RMS error has an increasing behavior with height. This is due to bias being introduced in the algorithm. NN algorithm used to retrieve the water vapor and temperature profiles has been trained using a data set taken from areas which have similar weather conditions as the radiometer observation site. However, two sites at the same altitude and longitude may have significantly different weather depending on the general conformation of the mountains in the area, the marine currents as well as the advection processes. This training of the algorithm is causing the retrieval bias for both the water vapor and temperature profiles. However, at high altitudes the range of water vapor density values which are possible are limited and close to zero (obviously the climatological mean) due to which the errors reduce as altitude increases as shown in Fig. 11a. This is not the case for temperature profiles, which can have really low values at high altitudes. If the training data have really low values of temperature at high altitudes for a set of brightness temperatures then the retrieved profile will also be low in comparison to the actual profile or the reanalysis data in this case. Thus as the altitude increases, the temperature profile error increases too.

5 Conclusion and discussion

This paper comprehensively describes the Bayesian optimal estimation and the improvements applied to the technique to estimate humidity and temperature profiles with increased accuracy. The Bayesian technique is an optimal combination of ground-based microwave radiometer observations and the related background information as well as the a-priori information. Hence, the background data set is one of the important parameters in improving accuracy and in increasing the ability to detect temporal changes and gradients. Therefore, the effect of using a small background data set has been studied in this paper. To that effect the Bayesian optimal estimation has been applied to the radiometer measurements performed for the month of August 2011 to retrieve water vapor density and temperature profiles while considering a data set taken for a period of 1 month. The retrieved profiles show that gradients can be detected along with temporal changes. These retrieved profiles have been compared with those from the NN method and also with the NOAA reanalysis data, which is considered as truth in this case. The results show that Bayesian optimal estimation using a small background information data set (50 profiles taken over a period of 1 month) has better performance than the NN method (which requires a large background data set taken over 4–5 years as training data), particularly when a large background data set is not available to train the NN method. This improved accuracy can be achieved because the profiles in the background data set are temporally and spatially correlated with the mea-

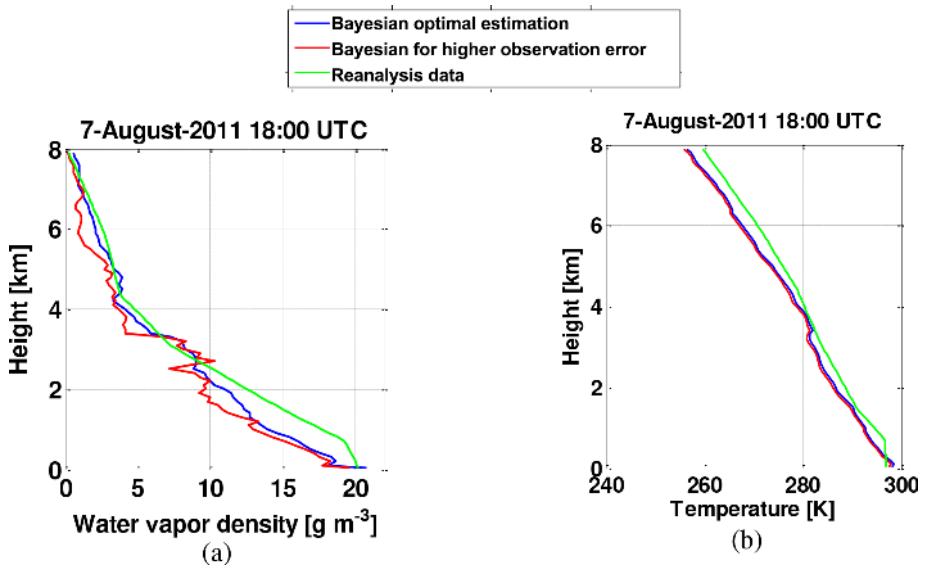

Figure 10. Retrieved profile sensitivity to observation error covariance matrix. **(a)** Water vapor profile. **(b)** Temperature profile.

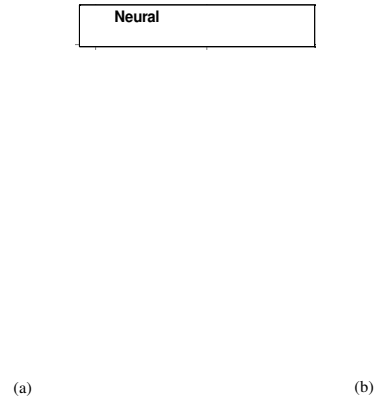

Figure 11. RMS error analysis for **(a)** water vapor profiles and **(b)** temperature profiles.

surements performed by the radiometer. Thus, the most persistent profile is retrieved and the Bayesian optimal estimation achieves the improved retrieval performances throughout the altitude of interest.

Water vapor profiles retrieved using the Bayesian optimal estimation technique (Fig. 6) compares well with the reanalysis data for 16 August 2011 and 26 August 2011 with differences less than 1.5 g m^{-3} for the whole profile and for other days the difference is lower than the error observed for NN from ground to 3 km altitude. For most of the days the absolute errors are less than 2 g m^{-3}. In addition to that retrieved profiles are able to detect the gradients in the water vapor profile which are otherwise smoothed by the reanalysis data. The RMS error analysis for Bayesian estimation shows that the RMS errors are less than 0.8 g m^{-3} from ground to 8 km altitude, which in turn is less than the errors observed for NN. Thus, the water vapor profile can be retrieved using Bayesian optimal estimation with an accuracy of better than 1.5 g m^{-3} for most of the cases. Temperature profiles retrieved using Bayesian optimal estimation have errors of less than 3 K in the lowest 5 km of troposphere when compared with the reanalysis data while the NN profiles usually have a difference of 3 K or more for the whole profile. However, on most of the days temperature profiles can be retrieved with an accuracy of better than 1.5 K while detecting the gradients. This has been again proved in the RMS error analysis in Fig. 11. The RMS error shows that Bayesian method has error less than 0.7 K while the NN has error higher than 2 K and increases as the altitude increases.

Along with other analyses, one has been performed to determine the sensitivity of retrieved profile accuracy to change in observation error covariance matrix. It has been observed that water vapor profile retrieved error increases by almost 1–2 g m^{-3} with an increase of 0.25 K^2 of the diagonal elements of the matrix. However, an increase of 0.25 K^2 of the diagonal elements of the temperature error covariance matrix results in an increase of error less than 0.8 K.

By analyzing the errors it can be concluded that water vapor and temperature profiles can be retrieved with improved accuracy using Bayesian optimal estimation. Along with the accuracy, the water vapor and temperature gradients and temporal changes can also be detected. When a large background data set is not available the Bayesian optimal estimation performs way better than the NN retrieval technique in terms of accuracy.

6 Data availability

The radiometer brightness temperature data is property of Indian Institute of Tropical Meteorology (IITM), Pune which is an autonomous organization under the Ministry of Earth Sciences, India. The data is not publicly available but can be availed by collaborating with IITM as well as sending a request to Dr. G. Pandithurai at pandit@tropmet.res.in. The Bayesian optimal estimated water vapor and temperature profiles data can be provided by the authors to the user based on the request. The NOAA reanalysis data is on NOAA website and can be easily accessed by the user.

Acknowledgement. Authors would like to thank Earth System Research Laboratory, National Oceanic and Atmospheric Administration (NOAA), for providing such an useful reanalysis data set, which helped in analyzing the error associated with the estimated profiles. We would also like to thank Xavier Bosch-Lluis for his important contributions and suggestions.

Edited by: F. Soldovieri
Reviewed by: three anonymous referees

References

Ali, M. M.: Cyclone, in: Remote Sensing Applications, edited by: Roy, P. S., Dwivedi, R. S., and Vijayan, D.: National Remote Sensing Centre, Hyderabad, India, 11, 273–282, 2009.

Cimini, D., Hewison, T. J., Martin, L., Güldner, J., and Marzano, F. S.: Temperature and humidity profile retrievals from ground based microwave radiometers during TUC, Meteor. Z., 15, 45–56, 2006.

Feltz, W. F., Howell, H. B., Knuteson, R. O., Woolf, H. M., and Revercomb, H. E.: Near continuous profiling of temperature, moisture, and atmospheric stability using the Atmospheric Emitted Radiance Interferometer (AERI), J. Appl. Meteorol., 42, 584–597, 2003.

Goldsmith, J. E. M., Blair, F. H., Bisson, S. E., and Turner, D. D.: Turn-key Raman lidar for profiling atmospheric water vapor, clouds, and aerosols, Appl. Opt., 37, 4979–4990, 1998.

Hewison, T. J.: 1D-VAR retrieval of temperature and humidity profiles from a ground-based microwave radiometer, IEEE Trans. Geosci. Remote Sens., 45, 2163–2168, 2007.

Iturbide-Sanchez, F., Reising, S. C., and Padmanabhan, S.: A miniaturized spectrometer radiometer based on MMIC technology for tropospheric water vapor profiling, IEEE Trans. Geosci. Remote Sens., 44, 2181–2193, 2007.

Leena, P. P., Dani, K. K., Nath, A. Sanap, S. D., Pandithurai, G., and Kumar, V. A.: Validation of ground-based microwave radiometer data and its application in verifying atmospheric stability over Mahbubnagar during 2011 monsoon and post-monsoon seasons, Int. J. Remote Sens., 36, 2920–2933, 2015.

Liebe, H. J., Hufford, G. A., and Cotton, M. G.: Propagation modeling of moist air and suspended water/ice particles at frequencies below 1000 GHz, AGARD 52nd Specialists' Meeting of the Electromagnetic Wave Propagation Panel, Chapter 3, 1993,

Liljegren, J. C.: Microwave Radiometer Profiler Handbook, https://www.arm.gov/publications/tech_reports/handbooks/mwrp_handbook.pdf (last access: 8 August 2016), Microwave Radiometer Profiler Handbook, 2002.

Marzano, F. S., Cimini, D., Memmo, A., Montopoli, M., Rossi, T., De Sanctis, M., Lucente, M., Mortari, D., and Di Michele, S.: Flower Constellation of Millimeter-Wave radiometers for Tropospheric monitoring at pseudogeostationary scale, IEEE Trans. Geosci. Remote Sens., 47, 3107–3122, 2009.

Needs, N. R.: Observing Weather and Climate from the Ground Up: A Nationwide Network of Networks. National Academies, Washington, DC, 2009.

National Research Council Committee on Developing Mesoscale Meteorological Observational Capabilities to Meet Multiple National Needs, Observing Weather and Climate from the Ground Up: A Nationwide Network of Networks, National Academies, Washington, DC, 2009.

Radiometrics corporation.: Profiler Operator's Manual, Boulder, CO, 2008.

Rao, T. N., Sunilkumar, K., and Jayaraman, A.: Validation of humidity profiles obtained from SAPHIR, on-board Megha-Tropiques, Special Section: Megha-Tropiques, Curr. Sci. India, 104, 1635–1642, 2013.

Rodgers, C. D.: Inverse Methods for Atmospheric Sounding: Theory and Practice, World Scientific, 2000.

Rosenkranz, P. W.: Absorption of Microwaves by Atmospheric Gases, Atmospheric remote sensing by microwave radiometry, Wiley-Interscience Publication, 37–90, 1993.

Rosenkranz, P. W.: Water Vapor Microwave Continuum Absorption: A Comparison Of Measurements And Models, Radio Sci., 33, 919–928, 1998.

Rosenkranz, P. W.: Retrieval of temperature and miosture profiles from AMSU-A and AMSU-B measurements, IEEE Trans. Geosci. Remote Sens., 39, 2429–2435, 2001.

Sahoo, S., Bosch-Lluis, X., Reising, S. C., and Vivekanandan, J.: Radiometric Information Content for Water Vapor and Temperature Profiling in Clear Skies between 10 and 200 GHz, IEEE J. Sel. Topics Appl. Earth Observ. Remote Sens., 8, 859–871, 2015a.

Sahoo, S., Bosch-Lluis, X., Reising, S. C., and Vivekanandan, J.: Optimization of Background Information and Layer Thickness for Improved Accuracy of Water-Vapor Profile Retrieval from Ground-Based Microwave Radiometer Measurements at K-band, IEEE J. Sel. Topics Appl. Earth Observ. Remote Sens., 8, 4284–4295, 2015b.

Scheve, T. M. and Swift, C. T.: Profiling atmospheric water vapor with a K-band spectral radiometer, IEEE Trans. Geosci. Remote Sens., 37, 1719–1729, 1999.

Solheim, F. S., Godwin, J. R., Westwater, E. R., Han, Y., Keihm, S. J., Marsh, K., and Ware, R.: Radiometric profiling of temperature, water vapor, and cloud liquid water using various inversion methods, Radio Sci., 33, 393–404, 1998.

Spuler, S. M., Repasky, K. S., Morley, B., Moen, D., Hayman, M., and Nehrir, A. R.: Field-deployable diode-laser based differential absorption lidar (DIAL) for profiling water vapor, Atmos. Meas. Tech., 8, 1073–1087, doi:10.5194/amt-8-1073-2015, 2015.

Susskind, J., Blaisdell, J. M., Iredell, L., and Keita, F.: Improved temperature sounding and quality control methodology using AIRS/AMSU data: The AIRS Science Team Version 5 Retrieval

Algorithm, IEEE Trans. Geosci. Remote Sens., 49, 883–907, 2011.

Trenberth, K. E., Fasullo, J., and Smith, L.: Trends and variability in column-integrated atmospheric water vapor, Clim. Dynam., 24, 741–758, 2005.

Wang, J. and Zhang, L.: Systematic errors in global radiosonde perceptible water data from comparisons with ground-based GPS measurements, J. Clim., 21, 2218–2238, 2008.

Westwater, E. R.: Ground-based microwave remote sensing of meteorological variables, Atmospheric Remote Sensing by Microwave Radiometry, 145–214, 1993.